

Rapid Intensification of a Sheared, Fast-Moving Hurricane over the Gulf Stream

LEON T. NGUYEN AND JOHN MOLINARI

Department of Atmospheric and Environmental Sciences, University at Albany, State University of New York, Albany, New York

(Manuscript received 21 October 2011, in final form 8 March 2012)

ABSTRACT

Hurricane Irene (1999) rapidly intensified from 65 to 95 kt (~ 33.4 to 48.9 m s⁻¹) in 18 h. During the rapid intensification (RI) period, the northeastward storm motion increased from 10 to 18 m s⁻¹, the ambient southwesterly vertical wind shear increased from 6–7 to 10–13 m s⁻¹, and the downshear tilt of the inner core vortex increased. The azimuthal wavenumber-1 asymmetric convection that developed was consistent with a superposition of shear-induced and storm motion-induced forcing for vertical motion downshear and ahead of the center. Although the diabatic heating remained strongly asymmetric, it was of sufficient intensity to dramatically increase the azimuthally averaged heating. This heating occurred almost entirely inside the radius of maximum winds, a region known to favor rapid warm core development and spinup of the vortex. It is hypothesized that asymmetric forcing from the large vertical wind shear and rapid storm motion were responsible for RI. An unanswered question is what determines whether the heating will develop within the radius of maximum winds. Extraordinarily deep cells developed in the inner core toward the end of the RI period. Rather than causing RI, these cells appeared to be an outcome of the same processes noted above.

1. Introduction

Although tropical cyclone track forecasts have improved substantially over the past couple decades, intensity forecasts have experienced no such improvement (Rappaport et al. 2009). Rapid intensification (RI) events are particularly problematic in that they are almost always missed by operational forecasts (Elsberry et al. 2007). Despite their lack of predictability, there are some environmental factors that are often associated with rapid intensification. These include (but are not limited to) the presence of low ambient vertical wind shear, high oceanic heat content, and deep convection symmetrically distributed about the center (Kaplan et al. 2010). However, rapidly intensifying tropical cyclones undergoing moderate to high ambient vertical wind shear and possessing a highly asymmetric convective structure have been documented in the literature (Reasor et al. 2009; Molinari and Vollaro 2010). The processes involved in asymmetric rapidly intensifying tropical cyclones have garnered increasing interest in the research community.

Ambient vertical wind shear can modulate the structure and intensity of tropical cyclones. Enhanced low-level convergence and vertical motion favor convection occurring preferentially downshear to the left of shear of tropical cyclones (e.g., Rogers et al. 2003; Braun and Wu 2007; Sitkowski and Barnes 2009). Typically in the inner core, convective cells initiate downshear of the center, are advected by the swirling wind left of shear, and eventually dissipate upshear (e.g., Heymsfield et al. 2001; Black et al. 2002; Reasor et al. 2009). This wavenumber-1 convective asymmetry has been seen in numerous observational (e.g., Corbosiero and Molinari 2003; Chen et al. 2006; Cecil 2007) and modeling studies (e.g., Frank and Ritchie 2001; Braun et al. 2006; Riemer et al. 2010) in both the inner core and outer rainband regions. The increased ambient vertical wind shear usually acts as a negative influence on tropical cyclone intensity through several hypothesized mechanisms: ventilation of the upper-level warm core (Frank and Ritchie 2001), increased stability due to a midlevel warm anomaly (DeMaria 1996), ventilation of the tropical cyclone core by midlevel dry air (Cram et al. 2007; Tang and Emanuel 2010), and reduction of boundary layer moist entropy by downdrafts (Riemer et al. 2010).

Several recent idealized modeling studies highlight the contribution of diabatic heating within the inner core of a tropical cyclone to the intensification process.

Corresponding author address: Leon T. Nguyen, Department of Atmospheric and Environmental Sciences, University at Albany/SUNY, ES-339B, 1400 Washington Ave., Albany, NY 12222.
E-mail: lnguyen@albany.edu

Nolan et al. (2007) found the kinetic energy efficiency of the vortex, defined by the ratio of energy retained as kinetic energy to the injected heat energy, to increase with decreasing radius. For a TC with a radius of maximum winds (RMW) of 50 km, they found convective heating occurring at a 40-km radius to be nearly twice as efficient at intensifying the vortex as heating occurring at an 80-km radius. Using a balanced vortex model, Vigh and Schubert (2009) found that diabatic heating within the high inertial stability region inside the RMW results in enhanced subsidence inside the radius of heating and rapid amplification of the warm core. Applying the Sawyer–Eliassen equation to a balanced vortex, Pendergrass and Willoughby (2009) found that diabatic heating within the RMW results in a rapid increase of swirling winds and a contraction of the RMW. Assuming that diabatic heating continually occurred within the RMW, vortex intensification became more efficient with decreasing RMW.

Although strong ambient shear often displaces convection away from the TC center, making it difficult for the above arguments to apply for most strong shear cases, there have been observed cases of convection occurring near the center and resulting in intensification of the vortex. Molinari and Vollaro (2010) documented the case of Tropical Storm Gabrielle (2001), which rapidly intensified in 13 m s^{-1} of shear. The downshear reformation of the circulation center and the development of an intense convective cell nearly collocated with the center were crucial to the storm's RI. Shelton and Molinari (2009) studied the short-term intensification of Claudette (2003) into a hurricane despite ambient vertical wind shear exceeding 10 m s^{-1} . The effects of diabatic heating close to the center in both of these cases apparently overcame the negative influences of the ambient vertical wind shear.

This study documents the rapid intensification of Hurricane Irene (1999), which intensified under increasing vertical wind shear and developed a highly asymmetric structure as a result. This case differs from the previously mentioned case studies in that Irene was better organized than both Gabrielle and Claudette: its RI began when it was a minimal hurricane, while the other two cases were marginal tropical storms. Also, Irene was rapidly translating and was tracking near the warm Gulf Stream during the RI period. The impact of all of these factors on the asymmetric structure and rapid intensification of Hurricane Irene will be evaluated.

2. Data sources and calculations

The data sources for this study include (i) U.S. Air Force reconnaissance data, (ii) Weather Surveillance Radar-1988 Doppler (WSR-88D) data, (iii) cloud-to-ground

lightning data from the National Lightning Detection Network (NLDN; Cummins and Murphy 2009), (iv) 6-hourly gridded analyses (1.125° resolution) from the European Centre for Medium-Range Weather Forecasts (ECMWF), (v) sea surface temperature data from the Advanced Very High Resolution Radiometer (AVHRR) aboard the National Oceanic and Atmospheric Administration (NOAA) polar-orbiting satellites, and (vi) ambient vertical wind shear estimates from the Statistical Hurricane Intensity Prediction Scheme (SHIPS) database (DeMaria et al. 2005).

Aircraft reconnaissance data included flight-level wind speed and direction, temperature, and D value at the 850-hPa level for all flights relevant to this study. The data represent 10-s averages outputted at 1-min resolution. During the RI period, dewpoint measurements after 0231 UTC 18 October were unavailable because they were unrealistically low (below 10°C) with virtually no spatial variation. The center of Irene was defined using the minimum D value following Molinari and Vollaro (2010). Cross sections of flight-level data are presented with respect to radius instead of time. Although flight paths are sometimes erratic near the center, cross sections shown here are restricted to those with relatively straight flight paths.

To calculate the storm-relative radial and tangential wind, the storm motion was subtracted from the total wind. The storm motion was calculated using centered time differencing over 6-h intervals. Since the storm-relative radial wind estimate is sensitive to the center position, a measure of the uncertainty was devised roughly following the work of Shelton and Molinari (2009). A sample of 1000 random azimuthal directions (0° – 360°) was constructed. The center position was then displaced by 10 km in each of the random azimuth directions. The root-mean-square differences in radial wind from these center shifts were calculated and are shown by the shaded region in the storm-relative radial wind plot. Storm-relative radial wind estimates that had a root-mean-squared difference of greater than 10 m s^{-1} were omitted because the uncertainty was too large for meaningful interpretation. The mean storm-relative tangential wind time series was computed by linearly interpolating data from the two radial legs composing each center pass to 1-km resolution and then averaging them.

Level-II and level-III WSR-88D data are archived at the National Climatic Data Center. Each radar scans approximately once every 5 min. Level-III base reflectivity data from the Wilmington and Morehead City, North Carolina, radar sites were available from the lowest (0.5°) elevation angle only out to a distance of 230 km. Level-II reflectivity and velocity data from multiple elevation angles were available out to a distance of 460 km

TABLE 1. Description of the distance from the radar and elevation of the center of the radar beam for various figures in this paper.

Radar site	Time (UTC) and date	Distance between TC center and radar (km)	Radar beam centerline height at TC center (km)	Fig. No.	
KLTX (Wilmington)	1914–2015 UTC 17 Oct	153.8–184.4	2.88–3.81	6a	
	2125–2225 UTC 17 Oct	116.1–130.8	1.89–2.25	6b	
	2335–0006 UTC 17–18 Oct	107.6–118.4	1.69–1.94	6c	
	2355–0006 UTC 17–18 Oct	109.7–111.7	1.74–1.78	8a	
	0121–0131 UTC 18 Oct	130.9–134.2	2.25–2.34	8b	
	KMHX (Morehead City)	0134–0234 UTC 18 Oct	109.7–138.2	1.74–2.45	6d
		0343–0443 UTC 18 Oct	93.6–102.7	1.38–1.58	6e
0558–0657 UTC 18 Oct		139.7–186.7	2.48–3.89	6f	
KRAX (Raleigh)		0623 UTC 18 Oct	315.9	9.23	11a
	0848 UTC 18 Oct	424.5	15.4	11b	

from Wilmington and Raleigh, North Carolina, but not from Morehead City.

WSR-88D radial velocity data have been used to diagnose various aspects of tropical cyclone structure, including wind speed, center position, divergence fields, and wind field asymmetries (e.g., Stewart and Lyons 1996; Lee et al. 1999). However, few instances of using radial velocity data to diagnose vortex tilt in tropical cyclones exist in the literature. Molinari and Vollaro (2010) used radial velocity data from a WSR-88D radar to diagnose a left-of-shear tilt of the outer vortex of Tropical Storm Gabrielle. The methodology used to diagnose vortex tilt in this paper follows that of Molinari and Vollaro (2010), and will be described in detail here. The radial velocity product of the WSR-88D radar shows the component of the wind going away from (outbound) or toward the radar site (inbound) (Klazura and Imy 1993). Winds perpendicular to the radar beam have zero radial velocity. This zero isodop denotes the dividing line between outbound winds and inbound winds. Given the presence of a tilted vortex and assuming that the direction of tilt is not in the same direction as the radar beam, the tilt can be seen if the zero isodop position changes with height. One directional component of vortex tilt can be diagnosed using this method: the component perpendicular to the line segment between the radar site and the TC center. As the storm moves with respect to the radar site, the directional component of vortex tilt diagnosed by the radar changes. It should be noted that the zero isodop of the lowest elevation angle may not necessarily intersect

the interpolated center position for two possible reasons: (i) the minimum D value position did not correspond to the wind center and (ii) the center position was slightly in error due to the fact that the radar time was in between aircraft center fixes. However, the difference is relatively small, with the maximum error of the center position on the order of 5 km.

Velocity aliasing can be a significant limitation of using level-II velocity data (Klazura and Imy 1993). Aliasing occurred when the velocities detected by radar exceeded the maximum unambiguous velocity of 64 kt ($1 \text{ kt} = 0.5144 \text{ m s}^{-1}$). The aliased velocities created some erroneous zero isodops, which were eliminated by an automated procedure that identified unrealistically sharp horizontal radial velocity gradients.

Base reflectivity data were composited about the storm center over a series of 1-h periods. These are intended to show the time evolution of the precipitation structure about the vortex, but with the limitation that individual cells are smoothed out. Another limitation is that as the storm moves with respect to the radar site, the average radar beam height through the storm varies. To maintain a relatively uniform beam height during the time period, composites over more than 1 h were not used.

Table 1 lists the radar site, time period, distance of Irene's center from the radar site, and the radar beam centerline height at Irene's center for select figures that display radar data. Radar reflectivity data from Raleigh were used at very large distances from the radar site of 316 and 425 km and radar beam centerline heights of

9 and 15 km. There exist a couple caveats regarding the use of reflectivity at such large distances. A radar beam samples a larger vertical cross section as it travels farther away from the radar site due to its increasing beamwidth (Fig. 3 in Klazura and Imy 1993). At the above distances, the vertical thickness of the radar beam ranges from about 5–7 km. Another common problem at these distances is radar attenuation (Zrnić and Ryzhkov 1999), but given the strength of the returns in this case, attenuation does not appear to be a concern.

To construct the radar reflectivity Hovmöllers, the data were first translated to storm-relative coordinates (Burpee and Black 1989). The data were then bilinearly interpolated to cylindrical coordinates, with radial resolution of 1 km and azimuthal resolution of 1°, roughly following the work of Corbosiero et al. (2005). Azimuthally averaged reflectivity is plotted only to the 60-km radius, where 1° azimuth is equivalent to 1.05 km.

Sea surface temperature (SST) data calculated from the AVHRR were produced by the Johns Hopkins University Applied Physics Laboratory. Monaldo (1997) describes the methodology used in estimating SST from NOAA AVHRR satellite data. A significant limitation is that SSTs cannot be estimated underneath regions of cloud cover. This made it difficult to determine the SSTs underneath Irene's track immediately prior to the storm's passing, as cloud cover obscured large portions of the track area. Also, there were no data available during 7–13 October. The latest date prior to Irene's passage that had quality SST estimates over the region of interest was 4 October, about two weeks in advance. The path of the Gulf Stream upstream of Cape Hatteras exhibits rather low variability compared to regions downstream (Auer 1987; Taylor and Stephens 1998) because it is well constrained by the continental shelf (Olson et al. 1983). As a result, the SST estimates from 4 October are assumed to approximately represent the SST environment Irene encountered two weeks later.

Ambient vertical wind shear estimates from the SHIPS database are available every 6 h and are calculated from the GFS analysis fields over a radius of 500 km around the center of the tropical cyclone (DeMaria and Kaplan 1994; DeMaria et al. 2005). An independent estimate of vertical wind shear over the same region was derived from the 1.125° resolution ECMWF gridded analyses.

3. Storm history and large-scale environment

The history of Hurricane Irene is given by Avila (2000). It was named a tropical storm around 1200 UTC 13 October in the western Caribbean. Irene steadily intensified while moving north, becoming a hurricane

over the Florida Straits at 0600 UTC 15 October. Irene crossed south Florida and emerged as a minimal hurricane off the east-central coast of Florida early on 16 October.

Figure 1 shows the subsequent path of Irene overlaid with SST and the locations of the radar sites used in this paper. Irene passed along the northwestern edge of the Gulf Stream, where SSTs neared 29°C. Table 2 shows estimates of 6-hourly storm motion and ambient vertical wind shear from SHIPS and ECMWF. Irene accelerated toward the northeast from a storm motion of near 8 m s⁻¹ at 1800 UTC 17 October to near 16 m s⁻¹ at 0600 UTC 18 October. The ambient southwesterly vertical wind shear increased early on 18 October, from 6–7 m s⁻¹ at 0000 UTC to 10–13 m s⁻¹ at 0600 UTC. Prior to 1800 UTC 17 October, the shear vector was rotated approximately 55° clockwise from the storm motion vector, but afterward both vectors became approximately aligned.

Operational forecasters at the NHC in real time expected the increase in ambient vertical wind shear to preclude intensification, but instead Irene underwent a period of rapid intensification while off the North Carolina coast between about 2200 UTC 17 October and 0800 UTC 18 October. Figure 2 shows the minimum central sea level pressure from U.S. Air Force reconnaissance and maximum sustained surface winds from NHC best track. From 0106–0757 UTC 18 October, the pressure fell at a 2.5 hPa h⁻¹ rate to a minimum of 958 hPa. The maximum sustained surface winds increased from 65 kt at 1200 UTC 17 October to 95 kt at 0600 UTC 18 October, meeting the 30 kt (24 h)⁻¹ threshold for rapid intensification (Kaplan and DeMaria 2003; Kaplan et al. 2010). Peak flight-level (850 hPa) winds dramatically increased from 65–70 kt late on 17 October to a maximum of 114 kt recorded at 0759 UTC 18 October. Although Irene may have intensified even further, there were no reconnaissance flights into the storm after that time, so this was considered the peak intensity.

The reason for the acceleration of storm motion and the increase in vertical wind shear becomes apparent in Fig. 3, which shows upper-tropospheric potential vorticity near the beginning and near the end of the rapid intensification period. A large, broad trough centered near the Great Lakes approached the storm on 17 October. This trough met the 200-hPa eddy angular momentum flux convergence criterion for trough interaction (Hanley et al. 2001) during all time periods from 0000 UTC 17 to 0000 UTC 18 October, a period that included the beginning of rapid intensification. As the trough approached, vertical wind shear increased and the storm accelerated northeastward as southwesterly winds increased over the

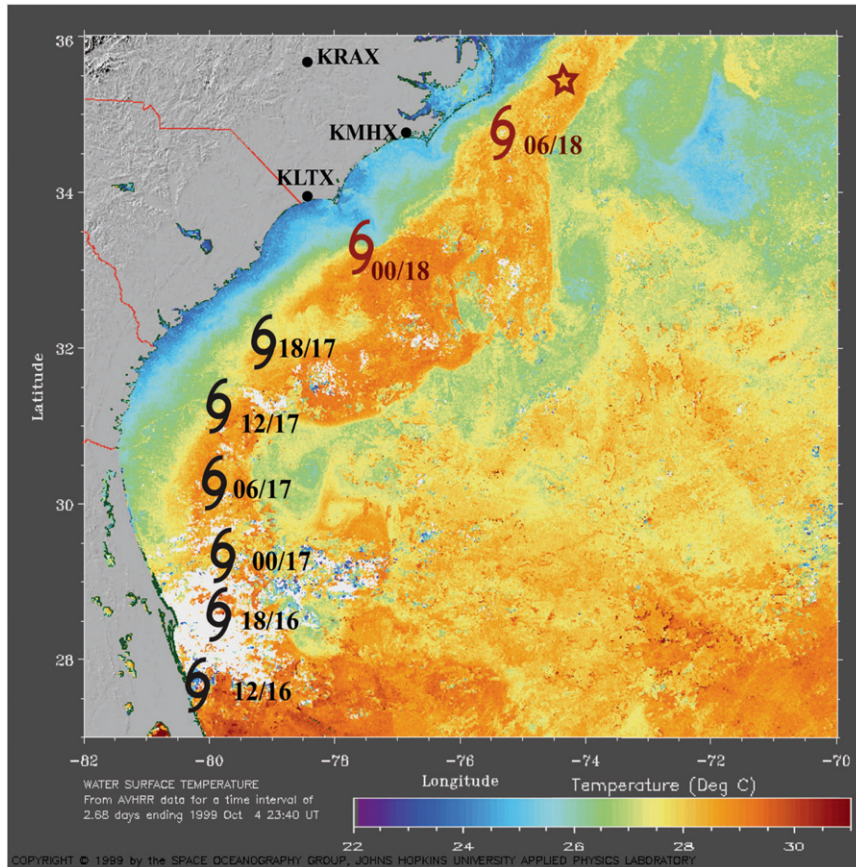


FIG. 1. Aircraft reconnaissance-based track at 6-h intervals (tropical cyclone symbols; times given in UTC hour/day format), the position of the center at peak intensity at 0757 UTC 18 Oct (star), and the three land-based radar locations. Symbols in red denote RI period. Mean SST ($^{\circ}\text{C}$, shading) for the period 2–4 Oct 1999 in the southern Gulf Stream region. The SST plot is courtesy of the Ocean Remote Sensing Group at Johns Hopkins University (images available online at <http://fermi.jhuapl.edu/avhrr/sst.html>).

storm. Because of the large distance (>400 km) between the center of the upper-level trough and Irene, the nature of the interaction between the two can be best described as a “distant interaction” (Hanley et al. 2001). The goals of this paper are to understand the nature of the rapid intensification during this period of increasing storm motion and vertical wind shear.

4. Vortex-scale evolution of Irene during rapid intensification

a. Flight-level observations of RI

Figure 4 shows the flight paths taken during the three reconnaissance flights used in Fig. 5. The 2117–2204 UTC 17 October and 0730–0825 UTC 18 October passes both

TABLE 2. Vertical wind shear and storm motion in Hurricane Irene. Shear is calculated between 850 and 200 hPa averaged within 500 km of the center from the SHIPS database (second column) and ECMWF gridded analyses (third column). Storm motion uses centered differencing over 6 h from the aircraft reconnaissance-based track.

Time	SHIPS vertical wind shear	ECMWF vertical wind shear	6-hourly storm motion
0000 UTC 17 Oct	227 $^{\circ}$ at 7.0 m s^{-1}	243 $^{\circ}$ at 7.9 m s^{-1}	187 $^{\circ}$ at 4.7 m s^{-1}
0600 UTC 17 Oct	227 $^{\circ}$ at 8.5 m s^{-1}	247 $^{\circ}$ at 11.3 m s^{-1}	187 $^{\circ}$ at 4.6 m s^{-1}
1200 UTC 17 Oct	233 $^{\circ}$ at 5.1 m s^{-1}	245 $^{\circ}$ at 6.5 m s^{-1}	187 $^{\circ}$ at 5.1 m s^{-1}
1800 UTC 17 Oct	211 $^{\circ}$ at 7.7 m s^{-1}	236 $^{\circ}$ at 5.7 m s^{-1}	228 $^{\circ}$ at 8.3 m s^{-1}
0000 UTC 18 Oct	224 $^{\circ}$ at 5.8 m s^{-1}	238 $^{\circ}$ at 7.3 m s^{-1}	233 $^{\circ}$ at 10.0 m s^{-1}
0600 UTC 18 Oct	233 $^{\circ}$ at 13.1 m s^{-1}	242 $^{\circ}$ at 10.4 m s^{-1}	232 $^{\circ}$ at 15.5 m s^{-1}
1200 UTC 18 Oct	237 $^{\circ}$ at 14.8 m s^{-1}	238 $^{\circ}$ at 11.4 m s^{-1}	237 $^{\circ}$ at 20.2 m s^{-1}

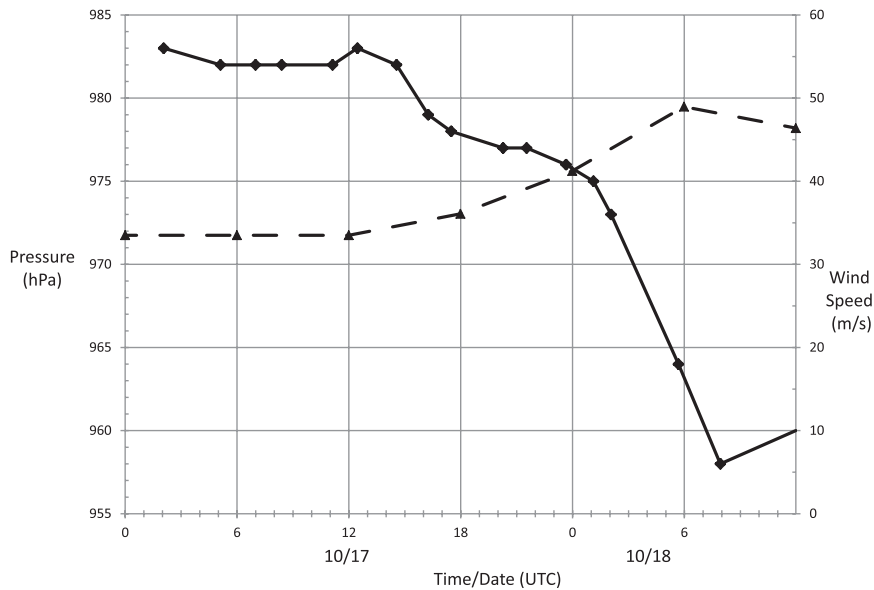


FIG. 2. (left) Minimum sea level pressure (hPa) as determined from aircraft reconnaissance (solid line) and (right) maximum sustained surface wind (m s^{-1}) at 6-h intervals from NHC best track (dashed line).

went through the center from approximately left of shear (and left of motion) to right of shear (right of motion). The 0138–0227 UTC 18 October pass approached the center from the upshear-left quadrant (left rear) and exited the center upshear (rear). Although these three passes do not all cover the same quadrants of the storm, they constituted the most linear flight paths during the RI period.

Figure 5a shows a cross section of 850-hPa storm-relative tangential wind for the three aircraft reconnaissance passes in Fig. 4. The storm-relative tangential wind profile during the 2134 UTC pass on 17 October was quite broad, with no clearly defined RMW. By 0205 UTC 18 October, storm-relative tangential winds increased close to the center, with the RMW located

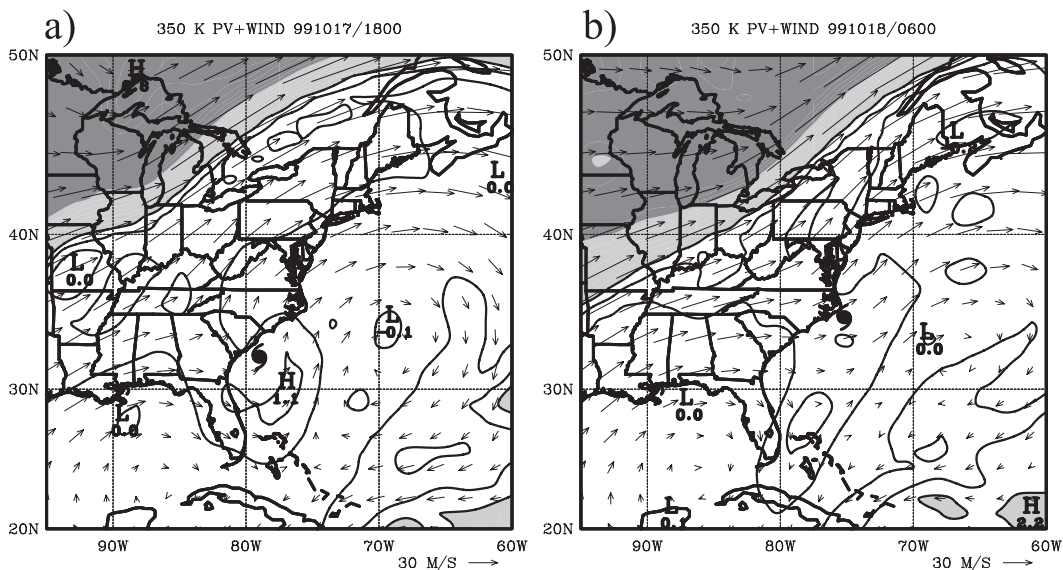


FIG. 3. Potential vorticity (PV) and winds on the 350-K isentropic surface, which lays around 200 hPa near the hurricane at (a) 1800 UTC 17 Oct and (b) 0600 UTC 18 Oct. PV is contoured at 0.5 potential vorticity unit (PVU) increments between 0–1.5 PVU ($1 \text{ PVU} = 10^{-6} \text{ m}^2 \text{ K s}^{-1} \text{ kg}^{-1}$). Light shading and dark shading represent 1.5–5 PVU and over 5 PVU, respectively.

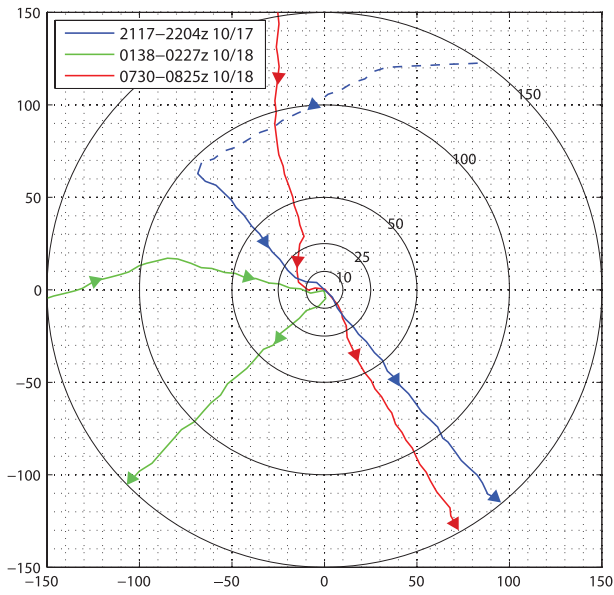


FIG. 4. Storm-relative flight tracks for the reconnaissance data cross sections plotted in Figs. 5, 6, and 10. The 2117–2204 UTC 17 Oct period is shown in blue, the 0138–0227 UTC 18 Oct period is shown in green, and the 0730–0825 UTC 18 Oct period is shown in red. Arrows denote the direction of travel. The blue dashed line denotes where data were omitted from the cross sections due to the rapidly changing azimuth from the center. Range rings denote 10-, 25-, 50-, 100-, and 150-km radii.

about 15 km in the west quadrant and at about 25 km in the southwest quadrant. By 0757 UTC 18 October, the storm-relative tangential winds had increased dramatically in the inner core, peaking at around 38 m s^{-1} about 10 km from the center. The ground-relative tangential winds at this time were very asymmetric because of the $16\text{--}20 \text{ m s}^{-1}$ storm motion (Table 2), with values in the south-southeast quadrant exceeding those in the north-northwest quadrant by a factor of more than 2 (see inset in Fig. 5a). Outside the 40-km radius, storm-relative tangential winds were observed to decrease by $3\text{--}5 \text{ m s}^{-1}$ from the earlier times.

The rapid intensification of the tangential wind field was accompanied by a large amplification of the 850-hPa temperature anomaly in the inner core (Fig. 5b). The 850-hPa temperature perturbation in the inner core was about 4°C during the 2134 UTC 17 October pass, 5°C near 0205 UTC 18 October, and 9°C near 0757 UTC 18 October. At peak intensity, the 850-hPa temperature profile showed both a broad low-amplitude warm anomaly extending out to the 150-km radius and a narrow 25-km-wide high-amplitude warm anomaly.

b. Wavenumber-1 convective asymmetry

Figure 6 shows a sequence of radar reflectivity 1-h composites from 1914 UTC 17 October (prior to RI) to

0657 UTC 18 October (1 h prior to peak intensity). In this discussion, “forward” and “rear” refer to the location with respect to storm motion. Prior to RI (Fig. 6a), reflectivity maxima were present outside the 50-km radius both downshear right (right forward) and upshear (rear) of the center. This latter maximum does not fit either the expected shear or motion-related maxima (Corbosiero and Molinari 2003). Over the next 2 h (Fig. 6b) several intensifying inner rainbands, comprising embedded convective cells, spiraled cyclonically inward around the north side (downshear left and left forward) of the center. These bands continued to wrap around the western and southern sides, and by 0000 UTC 18 October (Fig. 6c), the reflectivity structure around the center became more symmetric. Aircraft reconnaissance first observed an eye at 2340 UTC 17 October. This marked the beginning of an accelerated central pressure fall over the next 8 h. Outside the 50-km radius, the maximum reflectivity occurred in the northeastern (downshear and forward) half of the storm, consistent with the moderate southwesterly shear and 10 m s^{-1} northeastward storm motion (Table 2).

Although the symmetric precipitation structure near the center is characteristic of many rapid intensification events (Kieper 2010; Harnos and Nesbitt 2011), this structure was short lived. The ambient vertical wind shear and storm motion, both pointing to the northeast, increased substantially after 0000 UTC 18 October (Table 2). As a result, the reflectivity structure became more asymmetric, not only in the inner core but also in the inner and outer band regions. Figure 6d shows a reflectivity minimum resembling an eye with composite reflectivity exceeding 35 dBZ located downshear (forward) between 0134–0234 UTC 18 October. The radius of the highest composite reflectivity contracted to 10–15 km, while the RMW contracted to about 20 km (Fig. 5a). The eyewall asymmetry increased farther over the next 2 h (Fig. 6e), with the high reflectivity downshear to downshear-right (forward to right forward) forming a crescent-shaped band in the composite just 5–15 km from the center, while the upshear (rear) half became nearly devoid of precipitation. It is important to note in the individual radar scans (not shown), the convective band comprised numerous individual convective cells initiating approximately right of shear (right of motion), then being advected cyclonically into the downshear (front) quadrant, and finally dissipating left of shear and storm motion. At 0541 UTC 18 October, U.S. Air Force reconnaissance reported a closed eye of 6 km in diameter, which is tied for the third-smallest eye diameter ever recorded by U.S. Air Force reconnaissance (Vigh 2010). Even at this time the eyewall was highly asymmetric, with reflectivity exceeding 50 dBZ in the northeast (downshear

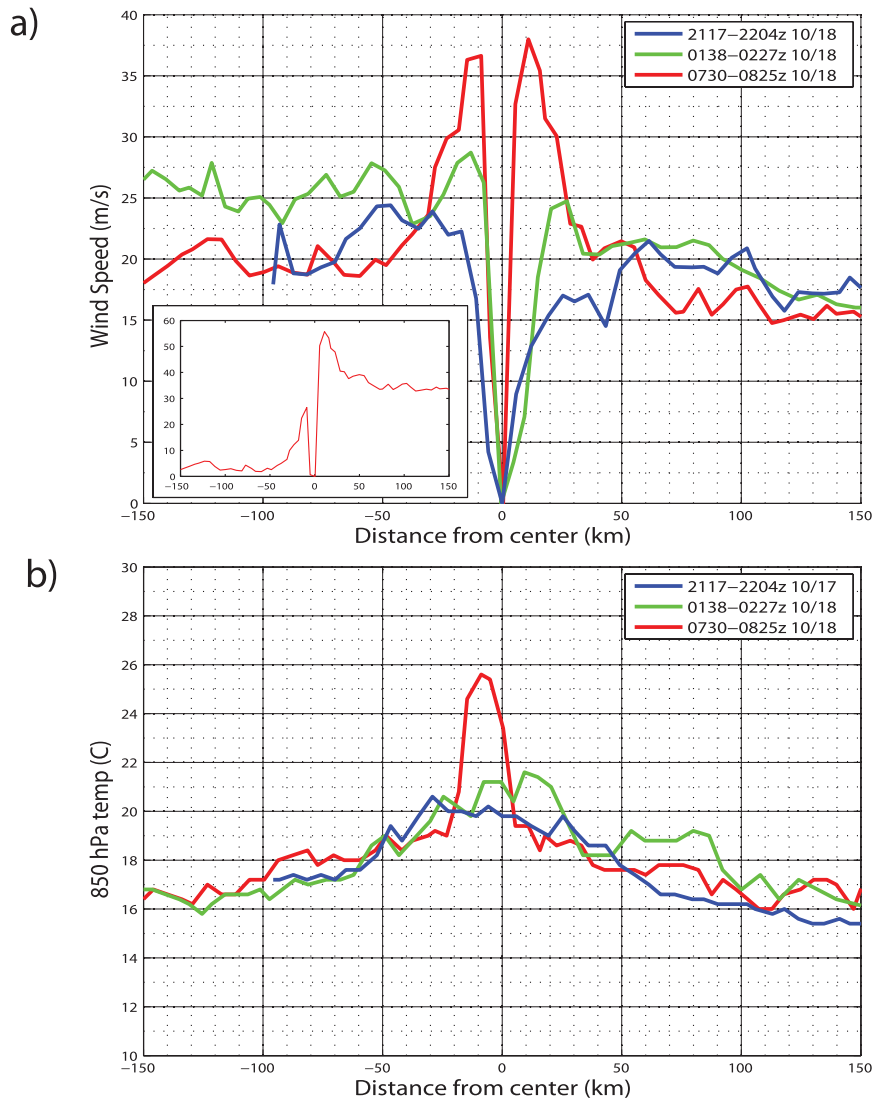


FIG. 5. U.S. Air Force reconnaissance cross section of (a) 850-hPa storm-relative tangential wind and (b) 850-hPa temperature for the three passes through the center shown in Fig. 4. The inset in (a) shows the ground-relative tangential wind during the 0730–0825 UTC 18 Oct pass. Ambient vertical wind shear is from the southwest.

and forward) quadrant but only near 25 dBZ in the southwest (upshear and rear) quadrant. Figure 6f shows that the eyewall opened up shortly thereafter, with strong reflectivity in the downshear-right (right front) quadrant between 10–20 km from the center and areas of weak or no reflectivity occurring upshear (rear) of the center. By this time, the ambient vertical wind shear was strong ($10\text{--}13\text{ m s}^{-1}$) and the storm motion was a brisk 16 m s^{-1} (Table 2).

Figure 7 shows an azimuth–time Hovmöller of radar reflectivity averaged over the 5–15-km radii. After 0230 UTC 18 October, reflectivity increased markedly and remained above 40 dBZ in the northeast quadrant

while reflectivity was much weaker in the southwest quadrant. This wavenumber-1 asymmetry is broadly consistent with numerous observational (e.g., Corbosiero and Molinari 2003; Chen et al. 2006; Abarca et al. 2011) and modeling studies (e.g., Frank and Ritchie 2001; Braun et al. 2006; Riemer et al. 2010) of tropical cyclones undergoing significant shear. A subtle difference is that Irene's favored convective region is located directly northeast (downshear) of the center as opposed to the downshear-left (northern) quadrant consensus in those studies. This may be partly attributed to the fast northeastward storm motion. Although the influence of vertical wind shear on convective asymmetries has been

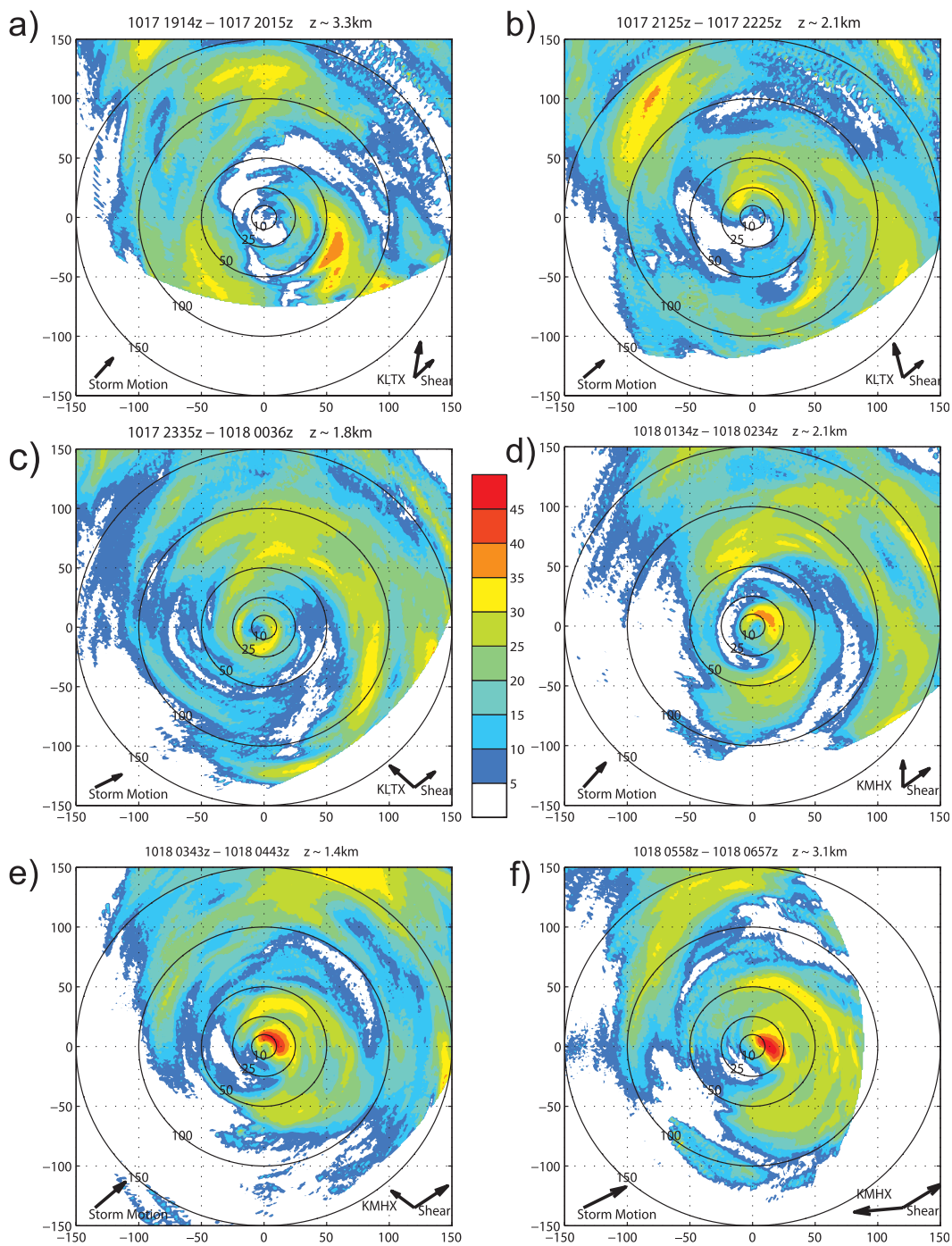


FIG. 6. WSR-88D radar reflectivity (dBZ) for the 0.5° elevation angle, composited about the storm center during the time ranges specified. (a),(b),(c) From the Wilmington, NC, radar; (d),(e),(f) from the Morehead City, NC, radar. Range rings represent distances of 10, 25, 50, 100, and 150 km from the tropical cyclone center. Average radar beam heights at the TC center during the composited time periods are shown at the top right of each. The shear vector and the approximate direction of the radar site relative to the center are shown at the bottom right of each. The storm motion vector is shown at the bottom left of each. The shear and storm motion vectors are scaled to magnitude.

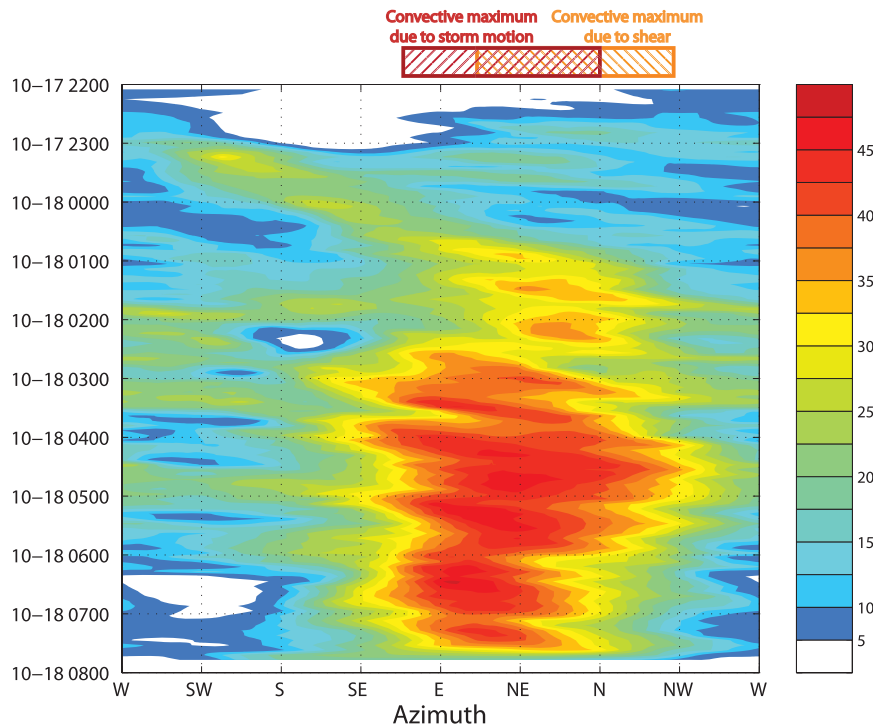


FIG. 7. Azimuth–time Hovmöller of Morehead City radar reflectivity averaged 5–15 km from the center between 2200 UTC 17 Oct and 0800 UTC 18 Oct. The orange and red hatched boxes denote the favored areas of convection by shear-induced and storm motion–induced forcing of vertical motion, respectively, following Corbosiero and Molinari (2003). The cross-hatched area denotes where the two overlap.

found to be substantially larger than that of storm motion (Corbosiero and Molinari 2003; Chen et al. 2006), Irene’s storm motion was large ($>15 \text{ m s}^{-1}$ after 0600 UTC 18 October) and may have played a more significant role in modulating convective asymmetries than what would typically be expected for tropical cyclones. Using a slab boundary layer model of constant depth, Shapiro (1983) found a maximum of boundary layer convergence in the right-front quadrant for a hurricane moving at 10 m s^{-1} . This was forced by an asymmetry in frictional drag due to stronger winds on the right. In comparing slab and height-resolving boundary layer models, Kepert (2010) found that slab boundary layer models overestimate storm motion–induced boundary layer inflow asymmetries, but the locations of the asymmetries in both models were similar. Although most observational studies have found a convective maximum to the front or right front of the center (e.g., Fig. 1 in Corbosiero and Molinari 2003; Chen et al. 2006; Abarca et al. 2011), these studies note that much of this signal may be attributable to the shear. In addition, Thomsen et al. (2012, manuscript submitted to *Quart. J. Roy. Meteor. Soc.*) using convection-permitting model simulations, found maximum upward motion to be in

the left-front quadrant. Although there remains some uncertainty, there is general agreement on maximum convection occurring in the front quadrants, with a slight preference to the right of motion. Figure 7 shows that the reflectivity maximum in the northeast quadrant in Irene is consistent with a combination of storm motion–induced and shear-induced forcing for vertical motion.

c. Evidence of vortex tilt

Figure 8 shows storm-relative zero isodop positions at three elevation angles. Near 0000 UTC 18 October (Fig. 8a), there appeared to be a substantial northeastward shift in the zero isodop with height outside of the 20-km radius (outer vortex). The outer vortex tilt was about 79° from the vertical axis. In contrast, there appeared to be very little shift in the zero isodop with height of the vortex within the 20-km radius (inner vortex). An hour and a half later (Fig. 8b), some inner-vortex tilt toward the north-northeast with height was diagnosed. The inner-vortex tilt was about 53° from the vertical axis. After this time, the center moved too far away from the radar site to evaluate vortex tilt.

Taking into account the constraints of only diagnosing one dimension of vortex tilt, it appears that the outer

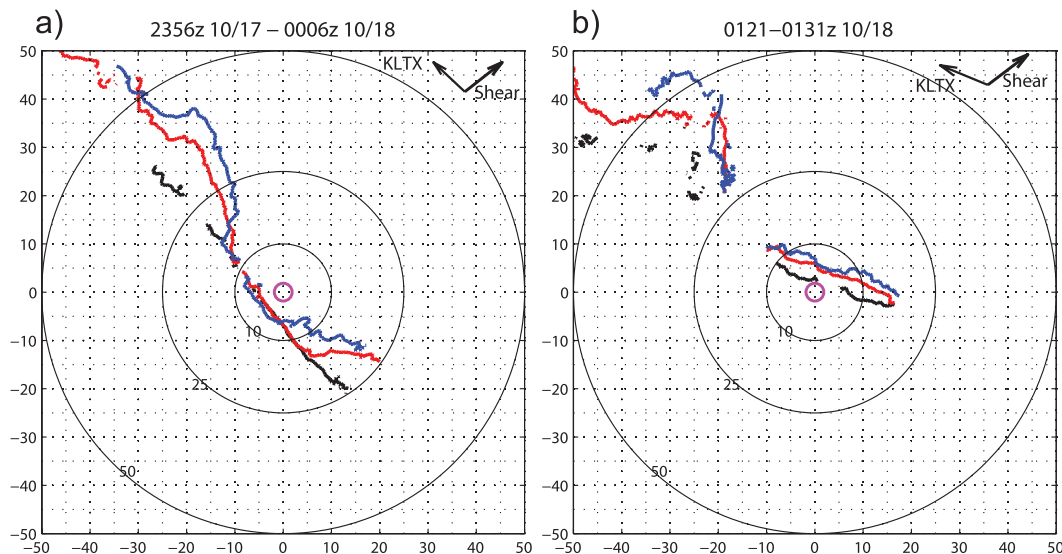


FIG. 8. Plot of the zero isodop position at the 0.5° (black), 1.5° (red), and 2.5° (blue) elevation angles derived from the radial velocity data from the Wilmington, NC, WSR-88D radar. The zero isodop position is composited relative to the storm center (denoted by the pink circle) over three radar times at (a) 2356 UTC 17 Oct, 0001 and 0006 UTC 18 Oct, and (b) 0121, 0126, and 0131 UTC 18 Oct. Range rings represent distances of 10, 25, and 50 km from the center. The x and y axes represent the zonal and meridional distance from the center. The shear vector and the direction of the radar site relative to the center are plotted at the top right of (a) and (b). The average height of the radar beam over the center in (a) is approximately 1.8 km (0.5° tilt), 3.7 km (1.5° tilt), and 5.5 km (2.5° tilt); and in (b) it is approximately 2.3 km (0.5° tilt), 4.8 km (1.5° tilt), and 7.1 km (2.5° tilt).

vortex tilt had a downshear component, and may have had a left-of-shear component as well. The inner vortex tilt at 0130 UTC 18 October had a downshear-left component. These results are in broad agreement with various model simulations (Braun et al. 2006; Riemer et al. 2010) and observations (Reasor and Eastin 2012) of sheared tropical cyclones, which indicate a generally downshear left or left of shear tilt. The greater magnitude of tilt of the outer vortex compared to the inner vortex is consistent with the results of Reasor et al. (2004) and Riemer et al. (2010).

The vortex tilt during this time appeared to evolve with the convective asymmetry shown in Figs. 6c,d. The tilt of the outer vortex and the lack of tilt of the inner vortex around 0000 UTC 18 October (Fig. 8a) are consistent with the wavenumber-1 asymmetry in reflectivity outside the 50-km radius and the relative axisymmetry of the eyewall reflectivity (Fig. 6c). About an hour and a half later, the emergence of an inner vortex tilt (Fig. 8b) occurs just prior to the development of significant wavenumber-1 asymmetry in the eyewall reflectivity (Fig. 6d), while the outer vortex tilt and wavenumber-1 asymmetry in reflectivity persist.

d. Asymmetric secondary circulation

Associated with the convective asymmetries in Fig. 6 was an increasing asymmetry in the secondary (in up

out) circulation, as observed from aircraft reconnaissance data. Figure 9 shows the 850-hPa storm-relative radial wind during two north-northwest–south-southeast (NNW–SSE) passes through the center: one just prior to the onset of RI and one at peak intensity. At the earlier time, storm-relative outflow of about $0\text{--}5\text{ m s}^{-1}$ was present to the NNW (left of shear and storm motion) and storm-relative inflow of about $5\text{--}10\text{ m s}^{-1}$ was present to the SSE (right of shear and storm motion) outside of 50 km. About 11 h later, the magnitude of both the storm-relative outflow and inflow increased to around $5\text{--}10$ and $10\text{--}20\text{ m s}^{-1}$, respectively. Other reconnaissance passes through the storm (not shown) indicate generally storm-relative inflow to the southeast and east of the center and storm-relative outflow to the north and west of the center. This outflow–inflow pair on opposite sides of the center was seen in flight-level observations of Claudette (2003), another storm that underwent strong ambient vertical wind shear (Shelton and Molinari 2009). Rather than increasing cross-storm flow, the anomalies in Fig. 9 suggest inflow into the strong upward motion region right of shear and outflow from the potentially subsident region left of shear. Evidence of the subsidence can be seen in the 0730–0825 UTC 18 October 850-hPa temperature profile shown in Fig. 5b. The maximum temperature anomaly observed at peak intensity was located about 10 km west-northwest

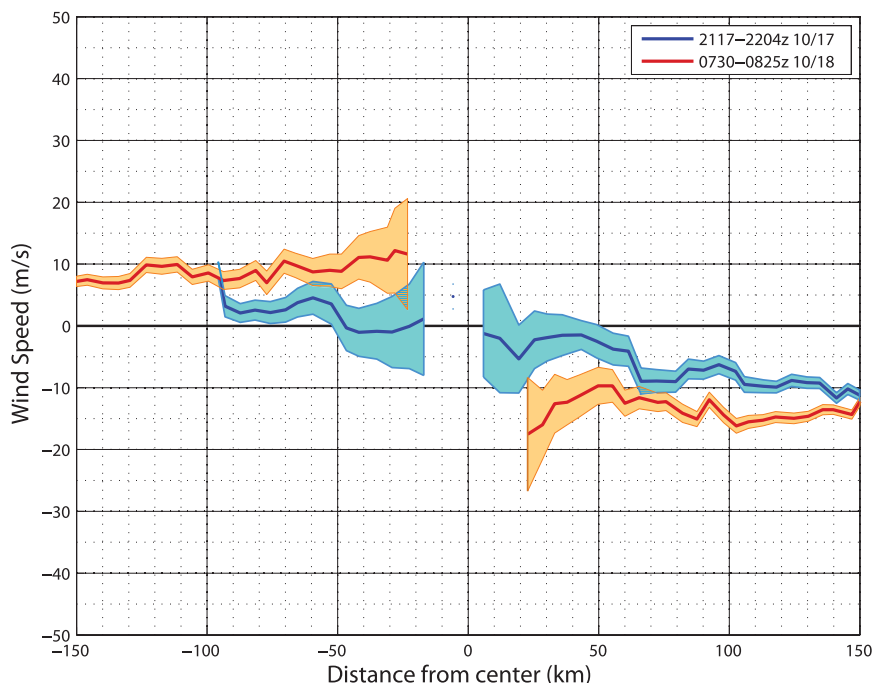


FIG. 9. U.S. Air Force reconnaissance cross section of flight-level (850 hPa) storm-relative radial wind for two separate passes through the center. Both passes were from approximately NNW (left of shear and motion) to SSE (right of shear and motion) of the center. The legend at the top right gives the time period. The shaded region indicates uncertainty in the radial wind determined by a series of random 10-km displacements of the storm center location. Regions where the uncertainty was too large for meaningful interpretation were omitted. See section 2 for methodological details.

(upshear left) of the center (Fig. 5b). The lack of precipitation in this region (Fig. 6f) suggests that adiabatic warming associated with subsidence may be responsible.

The increasing wavenumber-1 convective asymmetry, the presence of a tilted vortex, and the increasingly asymmetric secondary circulation suggest a vortex-scale response to the increasing ambient vertical wind shear and the accelerating storm motion after 0000 UTC 18 October. This is consistent with Rogers et al. (2003), who found that the low-level radial inflow, reflectivity, vortex tilt, and boundary layer divergence all varied consistently and nearly concurrently with the magnitude of the shear in simulations of Hurricane Bonnie (1998). Riemer et al. (2010) also showed in an idealized model a near-immediate response of the vortex's intensity and tilt to shear in their Figs. 3 and 5. However, this differs from the modeling results of Frank and Ritchie (2001), which found an approximately 12–24-h lag between the onset of shear and the subsequent tilting of the vortex in 15 m s^{-1} of shear, and even longer lags for lower shear magnitudes.

e. Azimuthally averaged reflectivity

Radius–time Hovmöllers of azimuthally averaged radar reflectivity and mean storm-relative tangential wind

are shown in Fig. 10. Prior to 2100 UTC 17 October (Fig. 10a), the azimuthally averaged reflectivity was weak ($<15 \text{ dBZ}$) within 40 km of the center, which is consistent with the reflectivity composite shown in Fig. 6a. Reflectivity slowly increased within the 40-km radius during the 2000–2300 UTC 17 October time period. Shortly after 2300 UTC 17 October, a $>27.5\text{-dBZ}$ azimuthally averaged reflectivity maximum developed 10–20 km from the center, well within the 50-km radius of maximum winds. This maximum coincided with the development of a closed eye seen in Fig. 6c and marked the beginning of an accelerated decrease in minimum central pressure. After 0100 UTC 18 October, the azimuthally averaged reflectivity from the Morehead City radar experienced a dramatic increase inside the radius of maximum winds (Fig. 10b). The azimuthally averaged reflectivity began to exceed 30 dBZ within 10 km at around 0300 UTC 18 October and reached a maximum of nearly 40 dBZ at 4–8 km from the center at 0500 UTC 18 October. The high reflectivities at the center in Fig. 10 are likely an artifact of the offset center position (see section 2). This increase in azimuthally averaged reflectivity was also observed from the Wilmington radar despite the increasing distance from that radar (Fig. 10a), indicating the increase of

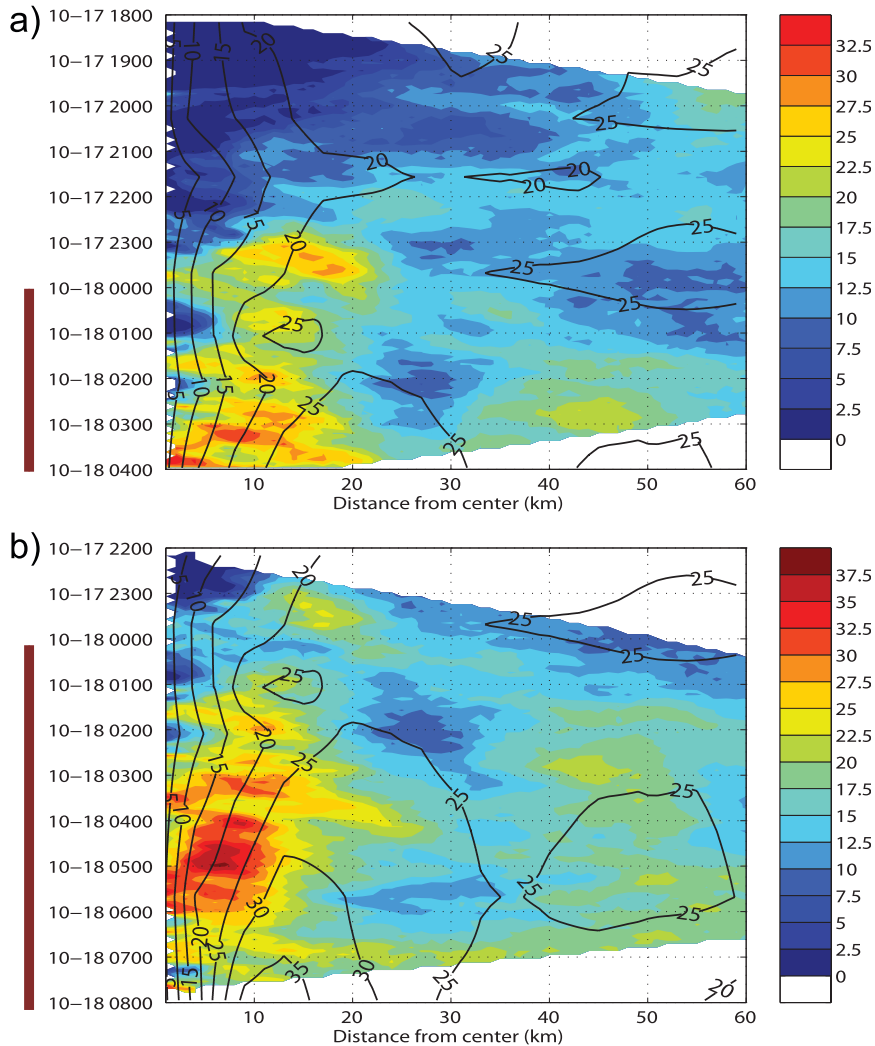


FIG. 10. Radius–time Hovmöller of azimuthally averaged radar reflectivity from (a) the Wilmington, NC, radar from 1800 UTC 17 Oct to 0400 UTC 18 Oct, and (b) the Morehead City, NC, radar from 2200 UTC 17 Oct to 0800 UTC 18 Oct. Mean storm-relative tangential wind (m s^{-1}) is shown in black contours. White areas denote where at least one data point along a given range ring around Irene’s center is outside radar range. Dark red bar on the left denotes the RI period. Irene’s center is closest to the radar sites in the middle of the images, and farthest away from the radar sites at the top and bottom.

reflectivity was due to heavier precipitation and not due to closer proximity to the radar. The azimuthally averaged reflectivity then decreased some after 0600 UTC 18 October, although that may be partially attributed to the distance between the center and the radar site (>160 km). Between 0300–0700 UTC 18 October, the reflectivity structure around the center of Irene was very asymmetric as a result of the increasing shear and storm motion (Figs. 6e,f and 7), but the strong reflectivities to the northeast of the center more than offset the weak reflectivities to the southwest, resulting in a large increase in the azimuthal average of reflectivity. Importantly, the

high azimuthally averaged reflectivity occurred almost entirely within the RMW (Fig. 10b), which was contracting from around 50 km at 0000 UTC to around 10 km by 0800 UTC 18 October.

Outward-propagating features were also observed in these radius–time Hovmöllers. In the Wilmington Hovmöller (Fig. 10a), the reflectivity maximum between 10–20 km shortly after 2300 UTC 17 October appeared to propagate outwards to the 20-km radius approximately a half-hour later. Other reflectivity maxima appeared to initiate within 5 km of the center at around 2345, 0130, and 0230 UTC and propagate outward at

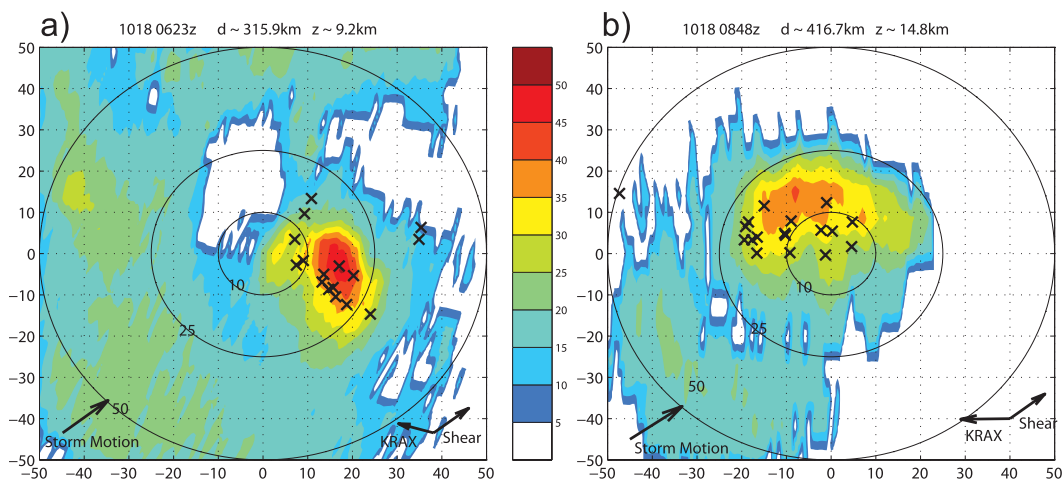


FIG. 11. Level-II reflectivity data from the Raleigh, NC, WSR-88D radar at the 0.5° elevation angle at two different times when extremely intense convective towers were present: (a) 0623 UTC 18 Oct and (b) 0848 UTC 18 Oct. Lightning flashes within 5 min of the radar scan are denoted by \times s. The radar direction relative to the TC center is given at the top left, as well as the vertical wind shear direction. The storm motion vector is shown at the bottom left. The shear and storm motion vectors are scaled to magnitude. The distance from the radar site and the average height of the radar beam at the center are given at the top. Range rings represent distances of 10, 25, and 50 km from the TC center.

approximately $20\text{--}25 \text{ km h}^{-1}$ ($5.6\text{--}6.9 \text{ m s}^{-1}$). Reflectivity minima appeared to initiate near the center at around 2200 and 0045 UTC and propagated outward to the 25–30-km radius at approximately 2300 and 0200 UTC, respectively. In the Morehead City Hovmöller (Fig. 10b), there appeared to be additional outward-propagating maxima that initiated within 5 km of the center at around 0300 and 0625 UTC. Corbosiero et al. (2006) also observed convective bands propagating outward at about 5.2 m s^{-1} in their radar study of intensifying Hurricane Elena (1985), and Abarca (2011) observed convective features propagating outward at similar speeds in several high-resolution WRF simulations. Abarca (2011) identified these features as azimuthal wavenumber-1 vortex Rossby waves. The origin of these outward-propagating features and their role in modulating the inner core structure of Irene are beyond the scope of this study.

5. Extremely intense convective towers

As the inner core convective structure became asymmetric after 0200 UTC 18 October, the intensity of the convection on the downshear half of the center increased as well. Several extremely intense convective towers developed in the inner core as Irene was reaching peak intensity between 0600–1000 UTC 18 October. During this time, the ambient vertical wind shear and forward motion were aligned and became quite large (Table 1). Figure 11 shows radar reflectivity at two different times from the

Raleigh radar, both at the lowest (0.5°) elevation angle. The Raleigh radar is shown here because its radar beam sampled a higher elevation, revealing the vertical depth of the convective towers. To account for the large vertical depth of the radar beam at such long ranges, the height of the top and bottom of the radar beam will be provided in this discussion in addition to the beam centerline height. Figure 11a shows that reflectivity in the convective tower around 0623 UTC reached 52 dBZ at a height of about 10.1 km (7.4–12.8 km). At 0848 UTC (Fig. 11b), reflectivity reached 43 dBZ at a height of about 14.8 km (11.4–18.2 km). At 0933 UTC, reflectivity reached 35 dBZ at a height of about 17.3 km (13.6–21.0 km) (not shown). All of these towers were located about 10–20 km from the center and were associated with lightning outbreaks. Infrared satellite imagery showed cloud tops of colder than -91°C (Beven and Stewart 2000). The spatial dimensions of each tower were approximately 10 km by 20 km. The position of the towers relative to the center shifted from downshear right (right forward) at 0623 UTC to left of shear and motion in the 0848 and 0933 UTC times. A similar counterclockwise progression of intense convective towers was seen in strongly sheared Tropical Storm Gabrielle (2001), which underwent a period of asymmetric rapid intensification (Molinari and Vollaro 2010).

The aforementioned reflectivities at the observed heights, even when using the height of the bottom of the radar beam, are extraordinary for a tropical cyclone. Cecil et al. (2002) constructed cumulative density functions of

reflectivities with height in tropical cyclones using 261 Tropical Rainfall Measuring Mission (TRMM) satellite overpasses. The 99.99th percentile height of the 52-, 43-, and 35-dBZ reflectivities in hurricane eyewalls were approximately 6, 8, and 12 km, respectively, all of which were easily surpassed in Irene. Although reflectivity derived from TRMM is not exactly equivalent to reflectivity from WSR-88D radars, correlations between the two range from 0.80–0.95 for levels above the bright band (Anagnostou et al. 2001). Heymsfield et al. (2010) also constructed cumulative density functions of reflectivity with height in seven tropical cyclones using data collected during several National Aeronautics and Space Administration (NASA) field experiments using the downward-looking *ER-2* Doppler Radar (EDOP). The average maximum height of the 50- and 40-dBZ reflectivities were 4.5 and 7 km, respectively, which also pale in comparison to the intense towers in Irene. Although such intense towers in tropical cyclones are rare, they have been observed in several case studies. An 18-km-tall tower was observed in the inner eyewall of Hurricane Bonnie (1998) by TRMM Precipitation Radar (Heymsfield et al. 2001), and reflectivity was observed to reach over 40 dBZ at 14 km in Hurricane Emily (2005) by the *ER-2* EDOP (Cecil et al. 2010). A convective tower 17 km deep in the genesis phase of Hurricane Ophelia (2005) was hypothesized to have been fueled by latent heat of freezing and high boundary layer moist entropy (Houze et al. 2009).

Intensification of tropical cyclones has been found to be associated with the development of extremely tall convective towers in the inner core (Kelley et al. 2004). In this case, the inner core convection intensified throughout the RI period, but did not achieve extreme intensity until Irene neared peak intensity. Thus, the extreme convective towers that occurred after 0600 UTC 18 October appeared to be a result of rather than a cause of RI.

6. Discussion

The development of intense convection near the center contributed significantly to the rapid intensification of Irene. Assuming that radar reflectivity can be used as an indicator of diabatic heating, the increase in azimuthally averaged heating within 5–10 km of the center (Fig. 10b) occurred inside the RMW, which was contracting from about 22 to 13 km during the period (Fig. 10). As noted earlier, diabatic heating within the RMW is most effective for producing intensification (Nolan et al. 2007; Vigh and Schubert 2009). In addition, intensification efficiency increases with decreasing RMW following the arguments of Pendergrass and Willoughby (2009). The narrow, high-amplitude warm core seen in Fig. 5b provides evidence of strong local subsidence adjacent to the heating region.

Although the magnitude of the wavenumber-1 convective asymmetry was increasing during rapid intensification (Figs. 6c–f and 7), the intense reflectivity to the northeast of the center more than offset the weak values to the southwest, resulting in the considerable increase in the azimuthal average shown in Fig. 10. The storm responded more to the azimuthal average of diabatic heating than to the degree of symmetry in diabatic heating, which is consistent with the results of Nolan et al. (2007) and Montgomery et al. (2006). These results parallel those of Reasor et al. (2009), who showed that ascent in the downshear-left quadrant of the eyewall was much stronger than upshear descent, resulting in large axisymmetric vertical motion and diabatic heating in the core of Hurricane Guillermo (1997).

Figure 12 shows a schematic diagram of the hypothesized influences on the rapid intensification of Hurricane Irene. Only the vicinity of the radius of maximum winds is shown. As the shear increased after 0000 UTC 18 October (Table 2), convective cells would be expected to initiate downshear right (e.g., Halverson et al. 2006; Braun and Wu 2007) and intensify as they moved into the downshear quadrant (e.g., Heymsfield et al. 2001). The rapidly accelerating storm motion from about 10 to 18 m s⁻¹ during the RI period (Table 2) ensures a clear signal in storm motion-induced asymmetries. As a result, the favored regions for upward motion based on previous work on vertical wind shear and storm motion overlapped in the northeast quadrant, exactly where the strongest convection developed (Figs. 6d–f and 7). An additional contributing factor may have been the enhanced surface enthalpy fluxes on the right side of the storm, where surface winds and SSTs associated with the Gulf Stream were likely higher (Fig. 1, inset in Fig. 5), but this is rather speculative given the lack of boundary layer observations.

The majority of storms experiencing ambient vertical wind shear above 10 m s⁻¹ do not intensify. One possible reason for this was provided by Riemer et al. (2010). The tilt of the outer vortex in a sheared storm induces an azimuthal wavenumber-1 asymmetry in convection outside the inner core, resulting in downward fluxes of low θ_e air into the inflow layer. Surface fluxes are insufficient to restore moist enthalpy as this air reaches the eyewall region, reducing the azimuthal-mean θ_e and weakening the storm (Tang and Emanuel 2010). In Hurricane Irene, a tilt of the outer vortex was observed (Fig. 8) as well as a corresponding region of convection downshear to downshear right outside the core and over the Gulf Stream, but the storm did not weaken. We speculate that large surface enthalpy fluxes from the Gulf Stream might have helped offset the negative influence of the downdrafts in the outer convective region.

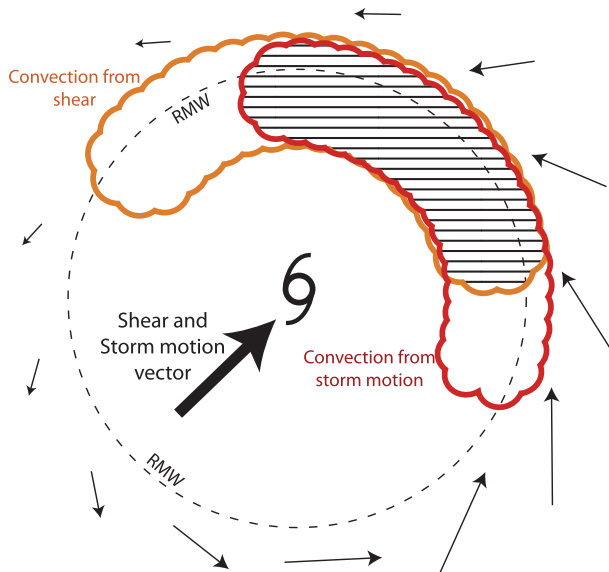


FIG. 12. Schematic diagram summarizing the interaction between the strong vertical wind shear and fast storm motion during the period of rapid intensification between 0000–0800 UTC 18 Oct. As in Fig. 7, convective areas favored by shear and storm motion are shown by the outlined area in orange and red, respectively, with the hatched region showing where they overlap. The dashed line represents the RMW. The straight arrows drawn outside the RMW represent the earth-relative surface winds (not drawn exactly to scale). The shear and storm motion vectors point approximately in the same direction and are denoted by the bold arrow near the center.

Although the azimuthal distribution of the convection during the RI is well explained by the effects of ambient vertical wind shear and fast storm motion, the radial distribution of the convection is not well accounted for. The occurrence of intense convection within the radius of maximum winds was vital for rapid intensification, but why the convection occurred so close to the center in the first place under a strong ambient vertical wind shear regime remains to be seen. Some strongly sheared tropical cyclones have a persistent area of convection occurring some 50–100 km away from the low-level circulation (Heymsfield et al. 2006); others have periodic convective bursts close to the center that can lead to temporary intensification followed by weakening (Shelton and Molinari 2009; Molinari and Vollaro 2010); while still others have persistent strong convection occurring around the center, forming either a band or an asymmetric eyewall and resulting in steady state or intensification (Heymsfield et al. 2001; Reasor et al. 2009). The ability to discriminate between tropical cyclones that respond to shear in each of these ways in real time remains one of the most difficult problems in operational intensity forecasting.

Acknowledgments. We thank Dr. Kerry Emanuel for his recommendation of the high-resolution AVHRR

SST data used in Fig. 1. We are indebted to David Vollaro for the programs used for shear and eddy angular momentum flux convergence calculations. We greatly appreciate the thorough and constructive comments from two anonymous reviewers. Gridded analyses from the ECMWF were obtained from NCAR, which is supported by the National Science Foundation (NSF). This work was supported by NSF Grant ATM0855718.

REFERENCES

- Abarca, S. F., 2011: Secondary eyewall formation in high resolution realistic hurricane simulations. Ph.D. dissertation, Department of Atmospheric and Oceanic Sciences, University of California, Los Angeles, Los Angeles, CA, 191 pp.
- , K. L. Corbosiero, and D. Vollaro, 2011: The World Wide Lightning Location Network and convective activity in tropical cyclones. *Mon. Wea. Rev.*, **139**, 175–191.
- Anagnostou, E. N., C. A. Morales, and T. Dinku, 2001: The use of TRMM Precipitation Radar observations in determining ground radar calibration biases. *J. Atmos. Oceanic Technol.*, **18**, 616–628.
- Auer, S. J., 1987: Five-year climatological survey of the Gulf Stream system and its associated rings. *J. Geophys. Res.*, **92** (C11), 11 709–11 726.
- Avila, L. A., cited 2000: Preliminary Report: Hurricane Irene 13–19 October 1999. National Hurricane Center. [Available online at <http://www.nhc.noaa.gov/1999irene.html>.]
- Beven, J. L., II, and S. R. Stewart, 2000: Mesoscale convective influences on the rapid intensification of Hurricane Irene (1999). Preprints, *24th Conf. on Hurricanes and Tropical Meteorology*, Fort Lauderdale, FL, Amer. Meteor. Soc., 14A.7. [Available online at https://ams.confex.com/ams/last2000/techprogram/paper_12743.htm.]
- Black, M. L., J. F. Gamache, F. D. Marks, C. E. Samsury, and H. E. Willoughby, 2002: Eastern Pacific Hurricanes Jimena of 1991 and Olivia of 1994: The effect of vertical shear on structure and intensity. *Mon. Wea. Rev.*, **130**, 2291–2312.
- Braun, S. A., and L. Wu, 2007: A numerical study of Hurricane Erin (2001). Part II: Shear and the organization of eyewall vertical motion. *Mon. Wea. Rev.*, **135**, 1179–1194.
- , M. T. Montgomery, and Z. Pu, 2006: High-resolution simulation of Hurricane Bonnie (1998). Part I: The organization of eyewall vertical motion. *J. Atmos. Sci.*, **63**, 19–42.
- Burpee, R. W., and M. L. Black, 1989: Temporal and spatial variations of rainfall near the centers of two tropical cyclones. *Mon. Wea. Rev.*, **117**, 2204–2218.
- Cecil, D. J., 2007: Satellite-derived rain rates in vertically sheared tropical cyclones. *Geophys. Res. Lett.*, **34**, L02811, doi:10.1029/2006GL027942.
- , E. J. Zipser, and S. W. Nesbitt, 2002: Reflectivity, ice scattering, and lightning characteristics of hurricane eyewalls and rainbands. Part I: Quantitative description. *Mon. Wea. Rev.*, **130**, 769–784.
- , K. R. Quinlan, and D. M. Mach, 2010: Intense convection observed by NASA ER-2 in Hurricane Emily (2005). *Mon. Wea. Rev.*, **138**, 765–780.
- Chen, S. S., J. A. Knaff, and F. D. Marks, 2006: Effects of vertical wind shear and storm motion on tropical cyclone rainfall asymmetries deduced from TRMM. *Mon. Wea. Rev.*, **134**, 3190–3208.

- Corbosiero, K. L., and J. Molinari, 2003: The relationship between storm motion, vertical wind shear, and convective asymmetries in tropical cyclones. *J. Atmos. Sci.*, **60**, 366–376.
- , —, and M. L. Black, 2005: The structure and evolution of Hurricane Elena (1985). Part I: Symmetric intensification. *Mon. Wea. Rev.*, **133**, 2905–2921.
- , —, A. R. Aiyyer, and M. L. Black, 2006: The structure and evolution of Hurricane Elena (1985). Part II: Convective asymmetries and evidence for vortex Rossby waves. *Mon. Wea. Rev.*, **134**, 3073–3091.
- Cram, T. A., J. Persing, M. T. Montgomery, and S. A. Braun, 2007: A Lagrangian trajectory view on transport and mixing processes between the eye, eyewall, and environment using a high-resolution simulation of Hurricane Bonnie (1998). *J. Atmos. Sci.*, **64**, 1835–1856.
- Cummins, K. L., and M. J. Murphy, 2009: An overview of lightning locating systems: History, technique, and data uses, with an in-depth look at the U.S. NLDN. *IEEE Trans. Electromagn. Compat.*, **51**, 499–518.
- DeMaria, M., 1996: The effect of vertical shear on tropical cyclone intensity change. *J. Atmos. Sci.*, **53**, 2076–2087.
- , and J. Kaplan, 1994: A Statistical Hurricane Intensity Prediction Scheme (SHIPS) for the Atlantic basin. *Wea. Forecasting*, **9**, 209–220.
- , M. Mainelli, L. K. Shay, J. A. Knaff, and J. Kaplan, 2005: Further improvements to the Statistical Hurricane Intensity Prediction Scheme (SHIPS). *Wea. Forecasting*, **20**, 531–543.
- Elsberry, R. L., T. D. B. Lambert, and M. A. Boothe, 2007: Accuracy of Atlantic and eastern North Pacific tropical cyclone intensity forecast guidance. *Wea. Forecasting*, **22**, 747–762.
- Frank, W. M., and E. A. Ritchie, 2001: Effects of vertical wind shear on the intensity and structure of numerically simulated hurricanes. *Mon. Wea. Rev.*, **129**, 2249–2269.
- Halverson, J. B., J. Simpson, G. Heymsfield, H. Pierce, T. Hock, and L. Ritchie, 2006: Warm core structure of Hurricane Erin diagnosed from high altitude dropsondes during CAMEX-4. *J. Atmos. Sci.*, **63**, 309–324.
- Hanley, D., J. Molinari, and D. Keyser, 2001: A composite study of the interactions between tropical cyclones and upper-tropospheric troughs. *Mon. Wea. Rev.*, **129**, 2570–2584.
- Harnos, D. S., and S. W. Nesbitt, 2011: Convective structure in rapidly intensifying tropical cyclones as depicted by passive microwave measurements. *Geophys. Res. Lett.*, **38**, L07805, doi:10.1029/2011GL047010.
- Heymsfield, G. M., J. B. Halverson, J. Simpson, L. Tian, and T. P. Bui, 2001: ER-2 Doppler radar investigations of the eyewall of Hurricane Bonnie during the Convection and Moisture Experiment-3. *J. Appl. Meteor.*, **40**, 1310–1330.
- , J. Simpson, J. Halverson, L. Tian, E. Ritchie, and J. Molinari, 2006: Structure of highly sheared Tropical Storm Chantal during CAMEX-4. *J. Atmos. Sci.*, **63**, 268–287.
- , L. Tian, A. J. Heymsfield, L. Li, and S. Guimond, 2010: Characteristics of deep tropical and subtropical convection from nadir-viewing high-altitude airborne Doppler radar. *J. Atmos. Sci.*, **67**, 285–308.
- Houze, R. A., W. Lee, and M. M. Bell, 2009: Convective contribution to the genesis of Hurricane Ophelia (2005). *Mon. Wea. Rev.*, **137**, 2778–2800.
- Kaplan, J., and M. DeMaria, 2003: Large-scale characteristics of rapidly intensifying tropical cyclones in the North Atlantic basin. *Wea. Forecasting*, **18**, 1093–1108.
- , —, and J. A. Knaff, 2010: A revised tropical cyclone rapid intensification index for the Atlantic and eastern North Pacific basins. *Wea. Forecasting*, **25**, 220–241.
- Kelley, O. A., J. Stout, and J. B. Halverson, 2004: Tall precipitation cells in tropical cyclone eyewalls are associated with tropical cyclone intensification. *Geophys. Res. Lett.*, **31**, L24112, doi:10.1029/2004GL021616.
- Keper, J. D., 2010: Comparing slab and height-resolving models of the tropical cyclone boundary layer. Part I: Comparing the simulations. *Quart. J. Roy. Meteor. Soc.*, **136**, 1689–1699.
- Kieper, M. E., 2010: Tropical cyclone morphology and phenomenology as depicted in passive microwave imagery. Preprints, *29th Conf. on Hurricanes and Tropical Meteorology*, Tucson, AZ, Amer. Meteor. Soc., 8B.4. [Available online at https://ams.confex.com/ams/29Hurricanes/techprogram/paper_168495.htm.]
- Klazura, G. E., and D. A. Imy, 1993: A description of the initial set of analysis products available from the NEXRAD WSR-88D system. *Bull. Amer. Meteor. Soc.*, **74**, 1293–1311.
- Lee, W., B. J. Jou, P. Chang, and S. Deng, 1999: Tropical cyclone kinematic structure retrieved from single-Doppler radar observations. Part I: Interpretation of Doppler velocity patterns and the GBVTD technique. *Mon. Wea. Rev.*, **127**, 2419–2439.
- Molinari, J., and D. Vollaro, 2010: Rapid intensification of a sheared tropical storm. *Mon. Wea. Rev.*, **138**, 3869–3885.
- Monaldo, F., cited 1997: Primer on the estimation of sea surface temperature using TeraScan processing of NOAA AVHRR satellite data, version 2.0 S1R-96M-03. Applied Physics Laboratory, The Johns Hopkins University. [Available online at <http://fermi.jhuapl.edu/>.]
- Montgomery, M. T., M. E. Nicholls, T. A. Cram, and A. B. Saunders, 2006: A vortical hot tower route to tropical cyclogenesis. *J. Atmos. Sci.*, **63**, 355–386.
- Nolan, D. S., Y. Moon, and D. P. Stern, 2007: Tropical cyclone intensification from asymmetric convection: Energetics and efficiency. *J. Atmos. Sci.*, **64**, 3377–3405.
- Olson, D., O. Brown, and S. Emmerson, 1983: Gulf Stream frontal statistics from Florida Straits to Cape Hatteras derived from satellite and historical data. *J. Geophys. Res.*, **88** (C8), 4569–4577.
- Pendergrass, A. G., and H. E. Willoughby, 2009: Diabatically induced secondary flows in tropical cyclones. Part I: Quasi-steady forcing. *Mon. Wea. Rev.*, **137**, 805–821.
- Rappaport, E. N., and Coauthors, 2009: Advances and challenges at the National Hurricane Center. *Wea. Forecasting*, **24**, 395–419.
- Reasor, P. D., and M. D. Eastin, 2012: Rapidly Intensifying Hurricane Guillermo (1997). Part II: Resilience in shear. *Mon. Wea. Rev.*, **140**, 425–444.
- , M. T. Montgomery, and L. D. Grasso, 2004: A new look at the problem of tropical cyclones in vertical shear flow: Vortex resiliency. *J. Atmos. Sci.*, **61**, 3–22.
- , M. D. Eastin, and J. F. Gamache, 2009: Rapidly intensifying Hurricane Guillermo (1997). Part I: Low-wavenumber structure and evolution. *Mon. Wea. Rev.*, **137**, 603–631.
- Riemer, M., M. T. Montgomery, and M. E. Nicholls, 2010: A new paradigm for intensity modification of tropical cyclones: Thermodynamics impact of vertical wind shear on the inflow layer. *Atmos. Chem. Phys.*, **10**, 3163–3188.
- Rogers, R., S. S. Chen, J. Tenerelli, and H. Willoughby, 2003: A numerical study of the impact of vertical shear on the distribution of rainfall in Hurricane Bonnie (1998). *Mon. Wea. Rev.*, **131**, 1577–1599.

- Shapiro, L. J., 1983: The asymmetric boundary layer flow under a translating hurricane. *J. Atmos. Sci.*, **40**, 1984–1998.
- Shelton, K. L., and J. Molinari, 2009: Life of a six-hour hurricane. *Mon. Wea. Rev.*, **137**, 51–67.
- Sitkowski, M., and G. M. Barnes, 2009: Low-level thermodynamic, kinematic, and reflectivity fields of Hurricane Guillermo (1997) during rapid intensification. *Mon. Wea. Rev.*, **137**, 645–663.
- Stewart, S. R., and S. W. Lyons, 1996: A WSR-88D radar view of Tropical Cyclone Ed. *Wea. Forecasting*, **11**, 115–135.
- Tang, B., and K. Emanuel, 2010: Midlevel ventilation's constraint on tropical cyclone intensity. *J. Atmos. Sci.*, **67**, 1817–1830.
- Taylor, A. H., and J. A. Stephens, 1998: The North Atlantic Oscillation and the latitude of the Gulf Stream. *Tellus*, **50A**, 134–142.
- Vigh, J. L., 2010: Formation of the hurricane eye. Ph.D. dissertation, Colorado State University, Fort Collins, CO, 538 pp.
- , and W. H. Schubert, 2009: Rapid development of the tropical cyclone warm core. *J. Atmos. Sci.*, **66**, 3335–3350.
- Zrnić, D. S., and A. V. Ryzhkov, 1999: Polarimetry for weather surveillance radars. *Bull. Amer. Meteor. Soc.*, **80**, 389–406.